Double Potential Well Regimes in Collisionless Spherical Discharges

Ryan M. Meyer, *Member, IEEE*, Sudarshan K. Loyalka, and Mark A. Prelas, *Member, IEEE*

***Abstract*—The study of potential profiles in glow discharges initiated between concentric spherical electrodes is motivated by the experimental investigations of inertial electrostatic confinement devices, which have the potential to be used as compact neutron generators. Here, we explore double potential well regimes within the cathode of such devices, utilizing a previously developed collisionless model. This is accomplished in an efficient manner by creating contour plots of the double well depth (DWD) and the double well radius, "width," with respect to the spreads in angular energy of electrons and ions, and with respect to the ion perveance and ratio of ion to electron perveance. These plots expand our knowledge of the DWD behavior beyond the previous understandings, both qualitatively and quantitatively. In addition, we consider the relationship of these results with the experimental results of Gu and Miley and the theoretical results of Matsuura *et al.* in an effort to better understand the results of Gu and Miley.**

***Index Terms*—Electrostatic discharges, inertial confinement, neutron sources.**

I. Introduction

THE STUDY of spherically symmetric glow discharges is inspired by an ongoing research on inertial electrostatic confinement (IEC). Our focus here is on the collisionless discharge regime such that $\lambda \gg d$, where λ is the mean free path of ions and d represents the diameter of the system's cathode. The existence of double potential wells in low-pressure spherically symmetric discharges has been noted in a recent paper [1], and the conditions for their existence will be further elucidated here.

Langmuir and Blodgett worked out a solution to Poisson's equation for a unipolar discharge between concentric spheres, assuming a monoenergetic source, and discovered the formation of deep potential wells [2]. Hirsch later computed a solution to the Poisson's equation for a bipolar spherical IEC (SIEC) discharge, also assuming the monoenergetic sources, and observed the formation of an infinite number of potential wells [3]. Lavrent'ev [4], Dolan [5], and Swanson *et al.* [6] sought more realistic models of SIECs by considering the distribution functions with finite widths. Swanson's results indicate the formation of the double potential well structures [7]. Meyer *et al.* [1] computed the potential profiles for a variety of spherical discharges, based on the prior model formulated by Lavrent'ev [4], Dolan [5], and Swanson *et al.* [6]. Matsuura *et al.* [8] explored the relationship between radial potential profile and neutron production rate. Their results do indeed indicate that a double well structure enhances the neutron production. Considering only the spherical discharge utilized in the more recent IEC research, Meyer *et al.* were able to compute a number of double potential well profiles [1]. The conclusions of Meyer *et al.* agree well with the SIEC modeling by Momota and Miley [9]. In addition, the results in [1] and [9] are generally in agreement with the stated conclusions of proton collimation experiments performed on an SIEC by Gu and Miley [10]. The general conclusions in [1], [8]–[10] with regard to the double potential well structures are the following.

1) A threshold ion perveance value $P_{\mathrm{i}}^{\mathrm{t}}$ exists for a given $\beta = P_{\mathrm{i}}/P_{\mathrm{e}}$, such that the double potential well structures exist for $P_{\mathrm{i}} > P_{\mathrm{i}}^{\mathrm{t}}$, where $P_{\mathrm{i}} = I_{\mathrm{i}}\varphi^{-3/2}$ is the ion perveance, $P_{\mathrm{e}} = I_{\mathrm{e}}\varphi^{-3/2}$ is the electron perveance, and I_{i}, I_{e}, and φ represent ion current, electron current, and electric potential, respectively.
2) Double well depth (DWD) increases monotonically as P_{i} is increased.
3) DWD increases as the relative focusing of electrons to ions improves.

This problem involves up to seven independent variables, and deciphering the dependence of the DWD on each of these can quickly become unwieldy. These variables include the spread in normalized electron angular energy $\sigma_{\mathrm{e},\phi}$, the spread in normalized ion angular energy $\sigma_{\mathrm{i},\phi}$, the spread in normalized electron total energy $\sigma_{\mathrm{e,E}}$, the spread in normalized ion total energy $\sigma_{\mathrm{i,E}}$, the ratio of ion perveance to electron perveance β, the ion perveance P_{i}, and the grid transparency η.

Our purpose in this paper is to analyze further the dependence of the DWD on these variables. Analysis can be simplified by reducing the number of independent variables under consideration. Results in [1] indicate that although the variation of the potential profile with $\sigma_{\mathrm{e,E}}$ and $\sigma_{\mathrm{i,E}}$ is not negligible, this variation is much less dramatic than the variation of the potential profile with the other five parameters. Thus, the effect of $\sigma_{\mathrm{e,E}}$ and $\sigma_{\mathrm{i,E}}$ on the potential profile is not considered here, and the computations are performed with $\sigma_{\mathrm{e,E}}$, and $\sigma_{\mathrm{i,E}}$ held at a constant value of 0.05. In addition, P_{i} and η are merged into a single variable known as the circulating ion perveance $P_{\mathrm{i}}^{\mathrm{C}} = ([2\,\eta]/[1-\eta^2])P_{\mathrm{i}}$.

We have explored the dependence of DWD in $\sigma_{\mathrm{e},\phi} - \sigma_{\mathrm{i},\phi}$ space and $\beta - P_{\mathrm{i}}^{\mathrm{C}}$ space. Contour plots are utilized to efficiently clarify the complexity of DWD on various combinations

Manuscript received September 7, 2006; revised December 21, 2006. This work was supported in part by the Missouri Space Grant Consortium (MSGC) Fellowship, the U.S. Department of Education's Graduate Assistance in the Area of National Need (GAANN) Fellowship, the University of Missouri-Columbia Huggin's Graduate Fellowship, and from the Innovations in Nuclear Education and Infrastructure (INIE).

The authors are with the Nuclear Science and Engineering Institute, University of Missouri-Columbia, Columbia, MO 65211 USA (e-mail: rmm346@mizzou.edu).

Digital Object Identifier 10.1109/TPS.2007.892734

of $\sigma_{e,\phi}$, $\sigma_{i,\phi}$, β, and P_i^C. We find that this presentation of data supports the previous qualitative understandings of the DWD behavior in SIEC devices. In addition, our explorations establish quantitative estimates of these qualitative attributes and expose new previously hidden qualitative trends.

In Section II, a brief physical description of the system being analyzed is provided. Next, a formal statement of the problem is given. In Section III, we provide a precise definition of DWD, present our results, and discuss the computations. Finally, in Section IV, the quantitative estimates of the previously known qualitative understandings will be highlighted, and the new qualitative understandings that can be gained from these data will be discussed. Finally, we discuss the implications that these results have and the simulations of Matsuura *et al.* [8] have, with respect to our interpretation of the proton rate profiles observed by Gu and Miley [10].

II. Problem Statement

The purpose is to compute the time independent radial potential profile $\varphi(r)$ for a bipolar spherical discharge, resembling an SIEC device in geometry. The cathode of such a device is a spherical grid with a geometric transparency of η. The cathode is located concentrically within a larger spherical anode. A discharge is initiated and sustained in the device by applying a high negative potential of several thousand volts to the cathode. The transparency of the cathode allows the ions to oscillate through the cathode a number of times given by the formula [11]

$$\#\text{ of ion orbits} = \frac{2\eta}{1-\eta^2}. \tag{1}$$

In the discussion to follow, the notation is used such that for an arbitrary parameter ψ, ψ_i implies that the parameter is associated with positive ions, while ψ_e implies it is associated with the electrons. The governing equations for this problem are the Poisson's equation

$$\nabla^2\varphi = -\frac{e}{\varepsilon_o}[n_i - n_e] \tag{2}$$

with equations of flux continuity

$$I_e = 4\pi r^2 e n_e v_e \tag{3}$$

and

$$I_i = 4\pi r^2 e n_i v_i \tag{4}$$

and the boundary conditions

$$\varphi(R_c) = \varphi_c$$

and

$$\nabla\varphi(0) = 0 \tag{5}$$

where φ is the electric potential at a point r, n is the number density, e is the charge of an electron, ε_o is the permittivity of free space, I is the current, v is the radial velocity, R_c is the cathode radius, and φ_c is the magnitude of the electric potential applied to the cathode. The combination of these results in the integro-differential equation

$$\frac{1}{r^2}\frac{d}{dr}\left[r^2\frac{d\varphi}{dr}\right] = \frac{1}{\varepsilon_o}\left[\rho_e(r,\varphi) - \rho_i(r,\varphi)\right] \tag{6}$$

where

$$\rho_i(r,\varphi) = \frac{1}{4\pi r^2}\left[\frac{m_i}{2e}\right]^{1/2} \cdot \int_{\varphi}^{0} dW_i \int_{0}^{\left[\frac{r^2}{R_c^2}\right][W_i-\varphi]} dS_i \frac{I_i(S_i,W_i)}{\left[W_i - \varphi - S_i\frac{R_c^2}{r^2}\right]^{1/2}} \tag{7}$$

and

$$\rho_e(r,\varphi) = \frac{1}{4\pi r^2}\left[\frac{m_e}{2e}\right]^{1/2} \cdot \int_{\varphi_c}^{\varphi} dW_e \int_{0}^{\left[\frac{r^2}{R_c^2}\right][\varphi-W_e]} dS_e \frac{I_e(S_e,W_e)}{\left[\varphi - W_e - S_e\frac{R_c^2}{r^2}\right]^{1/2}} \tag{8}$$

where S and W represent the angular and total energy, respectively, and ρ is the charge density. The following variables are normalized to aid in the numerical integration:

$$X = \frac{r}{R_c} \quad Y = -\frac{\varphi}{\varphi_c} \quad Y_{e,E} = -\frac{W_e}{\varphi_c}$$
$$Y_{i,E} = -\frac{W_i}{\varphi_c} \quad Y_{e,\phi} = \frac{S_e}{\varphi_c} \quad Y_{i,\phi} = \frac{S_i}{\varphi_c}. \tag{9}$$

The details of this solution for the following electron and ion Boltzmann distribution functions

$$I_e(Y_{e,\phi}, Y_{e,E}) = A_e e^{-(Y_{e,\phi}/\sigma_{e,\phi})} e^{([Y_{e,E}-1]/\sigma_{e,E})} \tag{10}$$

and

$$I_i(Y_{i,\phi}, Y_{i,E}) = A_i e^{-(Y_{i,\phi}/\sigma_{i,\phi})} e^{-(Y_{i,E}/\sigma_{i,E})} \tag{11}$$

are given in [1]. Here, A is a constant, σ_E is the spread in Y_E, and σ_ϕ is the spread in Y_ϕ. After normalizing the variables and simplifying the integrals represented in (7) and (8) for the distributions represented in (10) and (11), we arrive at

$$\frac{1}{X^2}\frac{d}{dX}\left[X^2\frac{dY}{dX}\right] = F_i(X,Y) - G_e(X,Y) \tag{12}$$

with

$$F_i(X,Y) = \frac{K_i}{X}\left[\frac{2\sigma_{i,E}\sigma_{i,\phi}^{3/2}}{\sigma_{i,\phi} - \sigma_{i,E}X^2}\right] \cdot \left[D\left(XY^{1/2}/\sigma_{i,\phi}^{1/2}\right) - X\{\sigma_{i,E}/\sigma_{i,\phi}\}^{1/2} D\left(Y^{1/2}/\sigma_{i,E}^{1/2}\right)\right] \tag{13}$$

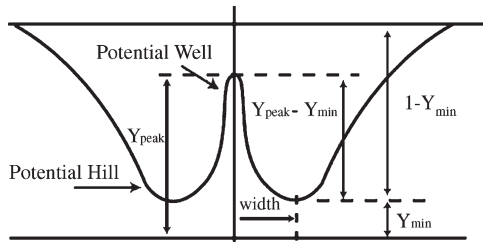

Fig. 1. Depiction of a double potential well solution. Note that Y has the opposite sign of the potential in practice due to the variable normalization.

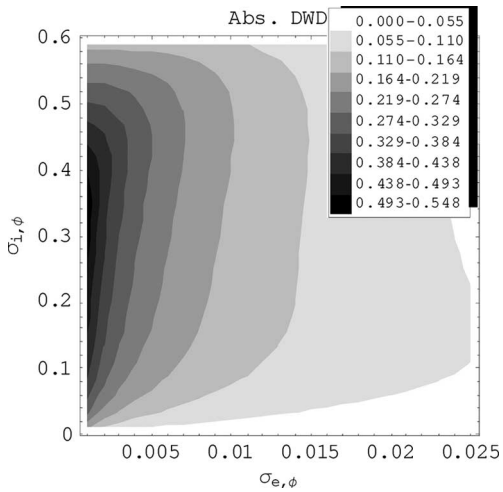

Fig. 2. Abs. DWD in $\sigma_{\mathrm{e},\phi}$–$\sigma_{\mathrm{i},\phi}$ space for ${}^{\mathrm{M}}P_{\mathrm{i}}^{\mathrm{C}} = 138$ mA $\cdot$ kV$^{-3/2}$ and ${}^{\mathrm{M}}\beta = 0.25$.

and

$$G_{\mathrm{e}}(X,Y) = \frac{K_{\mathrm{e}}}{X}\left[\frac{2\sigma_{\mathrm{e,E}}\sigma_{\mathrm{e},\phi}^{3/2}}{\sigma_{\mathrm{e},\phi}-\sigma_{\mathrm{e,E}}X^2}\right]\cdot\Big[D\Big(X[1-Y]^{1/2}/\sigma_{\mathrm{e},\phi}^{1/2}\Big) - X\{\sigma_{\mathrm{e,E}}/\sigma_{\mathrm{e},\phi}\}^{1/2}\,D\Big([1-Y]^{1/2}/\sigma_{\mathrm{e,E}}^{1/2}\Big)\Big]. \quad (14)$$

In (13) and (14)

$$K_{\mathrm{i}} = \big[2\eta/\{1-\eta^2\}\big] \cdot\Big[\{1/(4\pi\varepsilon_{\mathrm{o}}\sigma_{\mathrm{i,E}}\sigma_{\mathrm{i},\phi})\}\cdot\{m_{\mathrm{i}}/(2e)\}^{1/2}\Big] \cdot\Big[1-e^{-(1/\sigma_{\mathrm{i,E}})}-\{\sigma_{\mathrm{i},\phi}/(\sigma_{\mathrm{i},\phi}-\sigma_{\mathrm{i,E}})\} \cdot\Big\{e^{-(1/\sigma_{\mathrm{i},\phi})}-e^{-(1/\sigma_{\mathrm{i,E}})}\Big\}\Big]^{-1}\cdot\Big[I_{\mathrm{i}}/\varphi_c^{3/2}\Big] \quad (15)$$

$$K_{\mathrm{e}} = \big[2\eta/\{1-\eta^2\}\big] \cdot\Big[\{1/(4\pi\varepsilon_{\mathrm{o}}\sigma_{\mathrm{e,E}}\sigma_{\mathrm{e},\phi})\}\cdot\{m_{\mathrm{e}}/(2e)\}^{1/2}\Big] \cdot\Big[1-e^{([Y_{\min}-1]/\sigma_{\mathrm{e,E}})}+\{\sigma_{\mathrm{e},\phi}/(\sigma_{\mathrm{e},\phi}-\sigma_{\mathrm{e,E}})\} \cdot\Big\{e^{([Y_{\min}-1]/\sigma_{\mathrm{e},\phi})}-e^{([Y_{\min}-1]/\sigma_{\mathrm{e,E}})}\Big\}\Big]^{-1}\cdot\Big[I_{\mathrm{e}}/\varphi_c^{3/2}\Big] \quad (16)$$

$$\mathrm{D}(z) = \frac{\sqrt{\pi}}{2}e^{-z^2}\mathrm{Erf}i(z) \quad (17)$$

where $\mathrm{D}(z)$ is the Dawson function and $\mathrm{Erf}i(z)$ is the imaginary error function

$$\mathrm{Erf}i(z) = -i\mathrm{Erf}(iz) \quad (18)$$

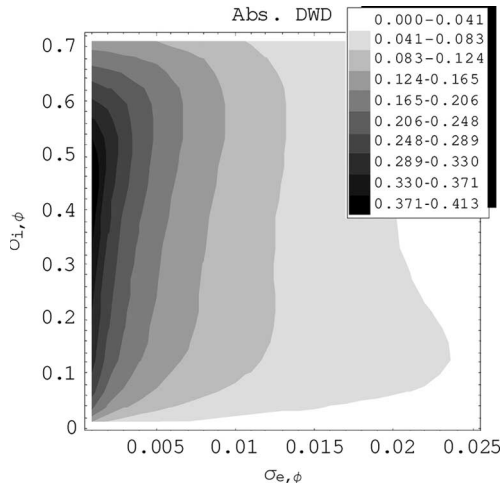

Fig. 3. Abs. DWD in $\sigma_{\mathrm{e},\phi}$–$\sigma_{\mathrm{i},\phi}$ space for ${}^{\mathrm{M}}P_{\mathrm{i}}^{\mathrm{C}} = 138$ mA $\cdot$ kV$^{-3/2}$ and ${}^{\mathrm{M}}\beta = 0.33$.

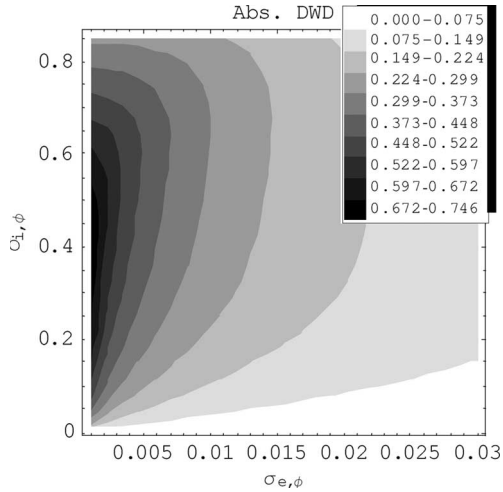

Fig. 4. Abs. DWD in $\sigma_{\mathrm{e},\phi}$–$\sigma_{\mathrm{i},\phi}$ space for ${}^{\mathrm{M}}P_{\mathrm{i}}^{\mathrm{C}} = 280$ mA $\cdot$ kV$^{-3/2}$ and ${}^{\mathrm{M}}\beta = 0.33$.

where $\mathrm{Erf}(x)$ is defined as

$$\mathrm{Erf}(x) = \int_0^x e^{-t^2}dt. \quad (19)$$

III. Computations and Results

In order to study the double well solutions for (12), it is convenient to develop precise definitions of the DWD and double well width. One definition is provided by Tzonev [12] and depicted in Fig. 1.

$$\text{Rel. DWD} = \frac{Y_{\mathrm{peak}}-Y_{\min}}{1-Y_{\min}}. \quad (20)$$

Equation (20) will be referred as the "Relative DWD," because the depth of the potential well is measured with respect to the height of the potential hill. Perhaps, more applicable to experiments is the "Absolute DWD," defined as follows:

$$\text{Abs. DWD} = Y_{\mathrm{peak}} - Y_{\min}. \quad (21)$$

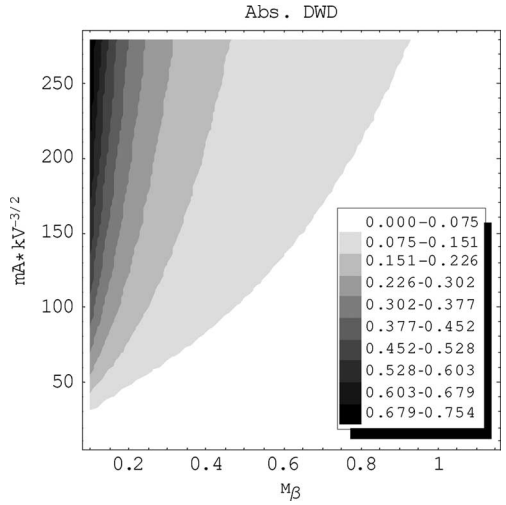

Fig. 5. Abs. DWD in ${}^{\mathrm{M}}\beta$–${}^{\mathrm{M}}P_{\mathrm{i}}^{\mathrm{C}}$ space for $\sigma_{\mathrm{e},\phi} = 0.003$ and $\sigma_{\mathrm{i},\phi} = 0.05$.

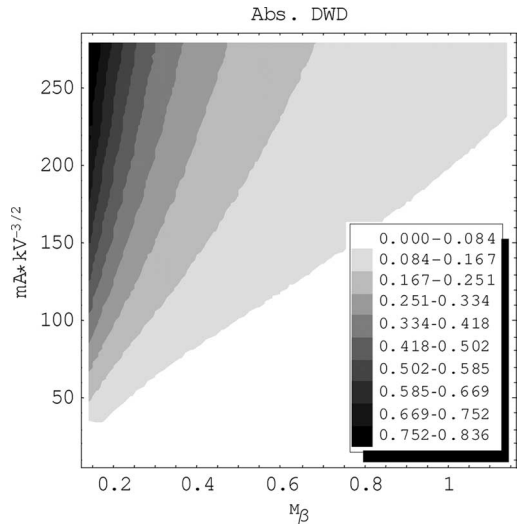

Fig. 6. Abs. DWD in ${}^{\mathrm{M}}\beta$–${}^{\mathrm{M}}P_{\mathrm{i}}^{\mathrm{C}}$ space for $\sigma_{\mathrm{e},\phi} = 0.003$ and $\sigma_{\mathrm{i},\phi} = 0.15$.

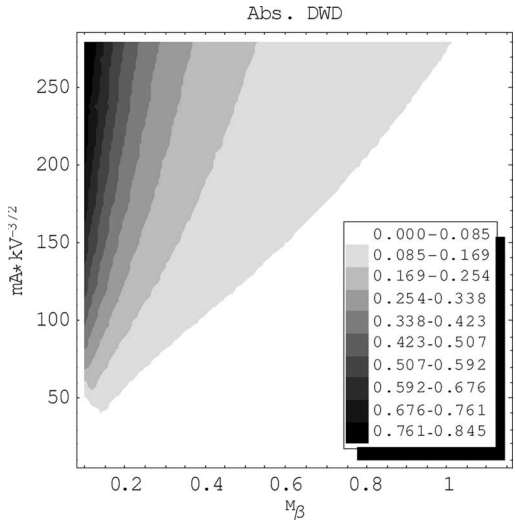

Fig. 7. Abs. DWD in ${}^{\mathrm{M}}\beta$–${}^{\mathrm{M}}P_{\mathrm{i}}^{\mathrm{C}}$ space for $\sigma_{\mathrm{e},\phi} = 0.005$ and $\sigma_{\mathrm{i},\phi} = 0.15$.

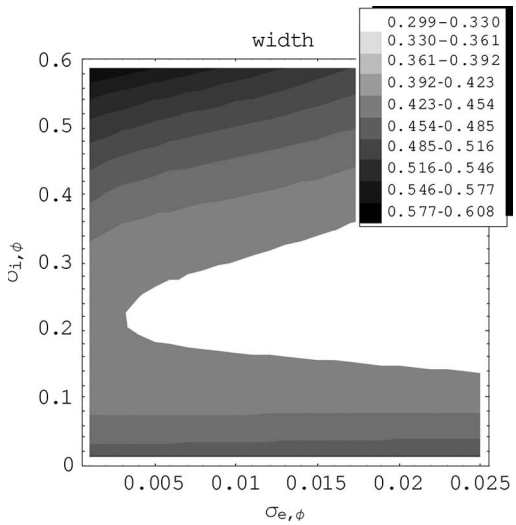

Fig. 8. Double well width in $\sigma_{\mathrm{e},\phi}$–$\sigma_{\mathrm{i},\phi}$ space for ${}^{\mathrm{M}}P_{\mathrm{i}}^{\mathrm{C}} = 138\ \mathrm{mA} \cdot \mathrm{kV}^{-3/2}$ and ${}^{\mathrm{M}}\beta = 0.25$.

The width of a double potential well is defined as the distance from the center of the device to the potential hill extrenum, as shown in Fig. 1.

The contours of Abs. DWD and width are plotted in $\sigma_{\mathrm{e},\phi}$–$\sigma_{\mathrm{i},\phi}$ space for two values of the "mass normalized" circulating ion perveance, ${}^{\mathrm{M}}P_{\mathrm{i}}^{\mathrm{C}} = P_{\mathrm{i}}^{\mathrm{C}}\ \mathrm{amu}^{1/2}$, and two values of the "mass normalized" β, ${}^{\mathrm{M}}\beta = \beta\ \mathrm{amu}^{1/2}$, where amu represents the mass of the ion species in atomic mass units. Contours of Abs. DWD and width are also plotted in ${}^{\mathrm{M}}\beta$–${}^{\mathrm{M}}P_{\mathrm{i}}^{\mathrm{C}}$ space for two values of $\sigma_{\mathrm{e},\phi}$ and two values of $\sigma_{\mathrm{i},\phi}$. The plots are with respect to ${}^{\mathrm{M}}P_{\mathrm{i}}^{\mathrm{C}}$ and ${}^{\mathrm{M}}\beta$ instead of $P_{\mathrm{i}}^{\mathrm{C}}$ and β to generalize the results with respect to ion specie mass.

Contour plots of Abs. DWD and width in the $\sigma_{\mathrm{e},\phi}$–$\sigma_{\mathrm{i},\phi}$ space for ${}^{\mathrm{M}}P_{\mathrm{i}}^{\mathrm{C}} = 138\ \mathrm{mA} \cdot \mathrm{kV}^{-3/2}$ are represented in Figs. 2 and 3 and Figs. 8 and 9, respectively. Figs. 2 and 8 show the results for ${}^{\mathrm{M}}\beta = 0.25$, while Figs. 3 and 9 show the results for ${}^{\mathrm{M}}\beta = 0.33$. The contours of Abs. DWD and width in $\sigma_{\mathrm{e},\phi}$–$\sigma_{\mathrm{i},\phi}$ space are displayed in Figs. 4 and 10 for ${}^{\mathrm{M}}P_{\mathrm{i}}^{\mathrm{C}} = 280\ \mathrm{mA} \cdot \mathrm{kV}^{-3/2}$ and ${}^{\mathrm{M}}\beta = 0.33$. Next, contours of Abs. DWD and width are plotted in the ${}^{\mathrm{M}}\beta$–${}^{\mathrm{M}}P_{\mathrm{i}}^{\mathrm{C}}$ space in Figs. 5–7 and Figs. 11–13, respectively. Figs. 5 and 11 display the contours for $\sigma_{\mathrm{e},\phi} = 0.003$ and $\sigma_{\mathrm{i},\phi} = 0.05$. Figs. 6 and 12 show the contours for $\sigma_{\mathrm{e},\phi} = 0.003$ and $\sigma_{\mathrm{i},\phi} = 0.15$, and finally, Figs. 7 and 13 display the contours for $\sigma_{\mathrm{e},\phi} = 0.005$ and $\sigma_{\mathrm{i},\phi} = 0.15$. The contours in Figs. 2–13 are generated from the grid points by interpolation with the third-order polynomials, and the computational statistics for these figures are shown in Table I.

In Figs. 2–4 and Figs. 8–10, the computations become more expensive as $\sigma_{\mathrm{i},\phi}$ and $\sigma_{\mathrm{e},\phi}$ become smaller. In addition, the solutions become increasingly difficult to compute for larger values of $\sigma_{\mathrm{i},\phi}$, more specifically, just beyond the large negative gradient that occurs in Abs. DWD with respect to $\sigma_{\mathrm{i},\phi}$. The regions along the ${}^{\mathrm{M}}\beta = 0.1$ in Figs. 5, 7, 11, 13 and ${}^{\mathrm{M}}\beta = 0.14$ in Figs. 6 and 12, are the most computationally expensive regions for these plots. In addition, as $\sigma_{\mathrm{e},\phi}$ is further decreased below 0.003, it becomes increasingly difficult to capture the entire Abs. DWD regimes in the ${}^{\mathrm{M}}\beta$–${}^{\mathrm{M}}P_{\mathrm{i}}^{\mathrm{C}}$ plane, as the expense of computing the left side of the Abs. DWD region becomes too great.

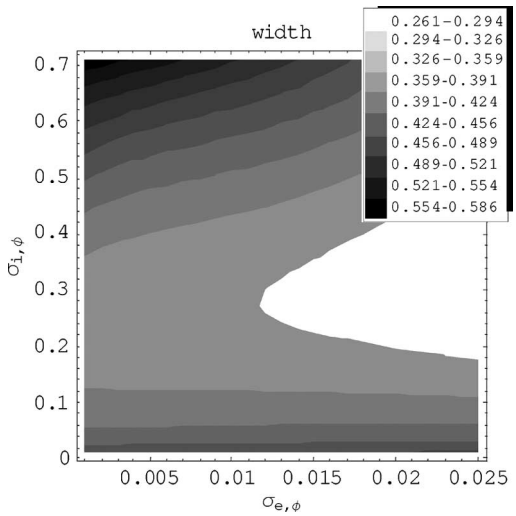

Fig. 9. Double well width in $\sigma_{e,\phi}$–$\sigma_{i,\phi}$ space for ${}^{M}P_{i}^{C} = 138\ \text{mA} \cdot \text{kV}^{-3/2}$ and ${}^{M}\beta = 0.33$.

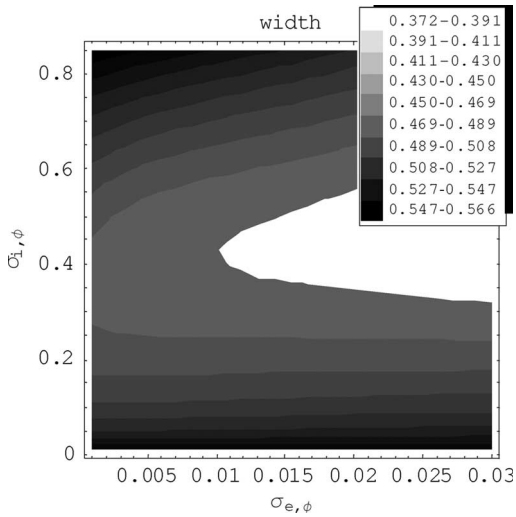

Fig. 10. Double well width in $\sigma_{e,\phi}$–$\sigma_{i,\phi}$ space for ${}^{M}P_{i}^{C} = 280\ \text{mA} \cdot \text{kV}^{-3/2}$ and ${}^{M}\beta = 0.33$.

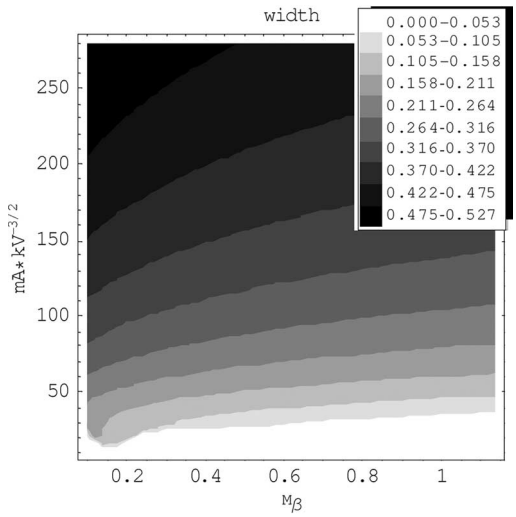

Fig. 11. Double well width in ${}^{M}\beta$–${}^{M}P_{i}^{C}$ space for $\sigma_{e,\phi} = 0.003$ and $\sigma_{i,\phi} = 0.05$.

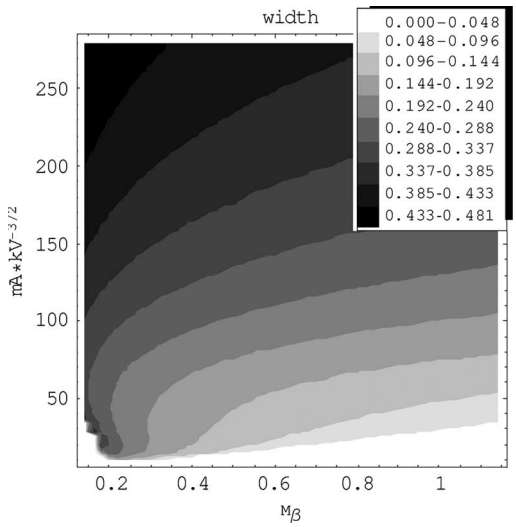

Fig. 12. Double well width in ${}^{M}\beta$–${}^{M}P_{i}^{C}$ space for $\sigma_{e,\phi} = 0.003$ and $\sigma_{i,\phi} = 0.15$.

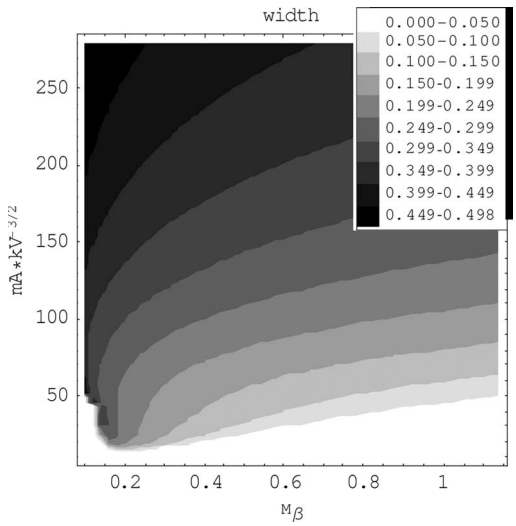

Fig. 13. Double well width in ${}^{M}\beta$–${}^{M}P_{i}^{C}$ space for $\sigma_{e,\phi} = 0.005$ and $\sigma_{i,\phi} = 0.15$.

IV. Discussion and Conclusion

The results presented here support the previous understandings of Abs. DWD behavior, provide quantitative estimates for these characteristics, and reveal new and previously unknown behavior. Figs. 2 through Fig. 4 support the previously stated conclusion that the DWD increases as the relative focusing of electrons to ions improves. These figures improve this understanding by revealing that this behavior exists only for small values of $\sigma_{i,\phi}$. In addition, they reveal that we can divide these plots into three regions according to the dependence of Abs. DWD on $\sigma_{i,\phi}$. The first region is located between the smallest value of $\sigma_{i,\phi}$ considered here $(\sigma_{i,\phi} = 0.01)$ and a critical value of $\sigma_{i,\phi}$ denoted as ${}^{c}\sigma_{i,\phi}$, beyond which, the previously discussed behavior diminishes. The second region is located between ${}^{c}\sigma_{i,\phi}$ and a second critical value of $\sigma_{i,\phi}$ denoted as ${}^{p}\sigma_{i,\phi}$, because it occurs at the value of $\sigma_{i,\phi}$ for which Abs. DWD peaks with respect to $\sigma_{i,\phi}$. In this region, Abs. DWD is less sensitive to $\sigma_{i,\phi}$. Finally, the third region is located above

TABLE I
COMPILATION OF STATISTICS FOR THE COMPUTATIONAL GRIDS UTILIZED IN FIGS. 2–13

Figure	x-axis	y-axis	x-axis MIN	x-axis MAX	y-axis MIN	y-axis MAX	x-axis grid spacing	y-axis grid spacing	# of grid pts.
Fig. 2, Fig. 8	$\sigma_{e,\emptyset}$	$\sigma_{i,\emptyset}$	0.001	0.025	0.010	0.590	0.00033	0.010	4307
Fig. 3, Fig. 9	$\sigma_{e,\emptyset}$	$\sigma_{i,\emptyset}$	0.001	0.025	0.010	0.710	0.00033	0.010	5183
Fig. 4, Fig. 10	$\sigma_{e,\emptyset}$	$\sigma_{i,\emptyset}$	0.001	0.030	0.010	0.850	0.00033	0.010	7480
Fig. 5, Fig. 11	${}^{M}\beta$	${}^{M}P_i^C$	0.10	1.14	10	280	0.020	3.0	4823
Fig. 6, Fig. 12	${}^{M}\beta$	${}^{M}P_i^C$	0.14	1.14	10	280	0.020	3.0	4641
Fig. 7, Fig. 13	${}^{M}\beta$	${}^{M}P_i^C$	0.10	1.14	10	280	0.020	3.0	4823

TABLE II
VALUES OF ${}^{c}\sigma_{i,\phi}$ AND ${}^{p}\sigma_{i,\phi}$ FOR FIGS. 2–4

	Fig. 2	Fig. 3	Fig. 4
${}^{c}\sigma_{i,\emptyset}$	0.15	0.15	0.25
${}^{p}\sigma_{i,\emptyset}$	0.5	0.6	0.7

${}^{p}\sigma_{i,\phi}$, and in this region, Abs. DWD declines dramatically with increasing $\sigma_{i,\phi}$. For a given value of $\sigma_{e,\phi}$, we can assign approximate values to ${}^{c}\sigma_{i,\phi}$ and ${}^{p}\sigma_{i,\phi}$ for each of the cases considered in Figs. 2–4, and these values are provided in Table II for $\sigma_{e,\phi} = 0.005$. Clearly, these values are not necessarily well defined, particularly ${}^{c}\sigma_{i,\phi}$, and a level of subjectiveness is involved in choosing the values from the plots. However, selecting these values allows one to at least qualitatively describe the effects of changing ${}^{M}\beta$ or ${}^{M}P_i^C$. For instance, from Table II, one can conclude that decreasing ${}^{M}\beta$ decreases ${}^{p}\sigma_{i,\phi}$ and an increase in ${}^{M}P_i^C$ increases ${}^{p}\sigma_{i,\phi}$. In addition, Table II shows that an increase in ${}^{M}P_i^C$ causes ${}^{c}\sigma_{i,\phi}$ to increase.

Fig. 5 through Fig. 7 support conclusions 1) and 2) of Section I. We can clearly see from these figures the monotonic relationship between Abs. DWD and ${}^{M}P_i^C$. Although a threshold may be defined in several ways, we can also conclude from Figs. 5–7 that, given a particular ${}^{M}\beta$, a threshold exists with respect to ${}^{M}P_i^C$ for double potential well formation. Considering that the double potential well formation is a consequence of the bipolar nature of the discharge, then one could expect to find an optimum value of ${}^{M}\beta$ with respect to the double potential well formation. This is illustrated near the lower right corners of Figs. 6 and 7. In addition, Fig. 7 indicates that this optimum value of ${}^{M}\beta$ drifts to lower values of ${}^{M}\beta$ as ${}^{M}P_i^C$ increases. It also appears from Figs. 5–7 that the optimum value of ${}^{M}\beta$ shifts to greater values of ${}^{M}\beta$ with increases in $\sigma_{i,\phi}$.

We now consider the relationship between Figs. 2–13, the data of Gu and Miley [10], and the results of Matsuura *et al.* [8]. Gu and Miley [10] constructed a high-resolution proton collimator to count the protons resulting from the fusion reactions in an operating SIEC filled with D_2 at a pressure of 1–10 mtorr. They were then able to back calculate the radial potential distribution from the counted protons. Their experiments were performed in the "starmode" discharge regime. "Starmode" occurs for suitable combinations of cathode grid geometry, cathode potential, and the plasma state, resulting in the formation of tightly collimated electron beams and ion beams [10]. This beamlike behavior indicates that the ions and electrons have a small σ_ϕ, and it means that the charged particles are focused toward the center of the cathode grid holes, away from the grid wire. Thus, from a charged particle's perspective, the cathode grid possesses a greater transparency η_{eff} than the grid's geometric transparency η ($\eta \sim 0.9$, typically).

To compare our results to the data of Gu and Miley [10], it is necessary to make reasonable estimates of the parameters considered here ($\sigma_{i,\phi}$, $\sigma_{e,\phi}$, β, and P_i^C). To account for this beamlike behavior, it is assumed that $\sigma_{i,\phi} \leq 0.05$ and that the effective transparency η_{eff} is greater than 98%. The range of $\sigma_{e,\phi}$ found in Figs. 2–4 and Figs. 8–10 cannot be directly reconciled with a collisional behavior because the electron distribution would broaden toward a Maxwellian in that case. β is probably the most difficult parameter to provide an estimate for, as it is likely to depend on the specific device, and the operating conditions. We do not attempt to estimate β here, and the values of β utilized in Figs. 2–13 are merely chosen for convenience.

Gu and Miley [10] report that a double potential well structure with Abs. DWD $= 0.22$–0.27 exists at $P_i = 1.38$ mA $\cdot$ kV$^{-3/2}$ which corresponds to the values of ${}^{M}P_i^C = 138$, and 276 mA $\cdot$ kV$^{-3/2}$ for $\eta_{\text{eff}} = 98\%$, and 99%, respectively. These values can be obtained by using η_{eff}, instead of η, in (1). Given the constraint imposed on $\sigma_{i,\phi}$ ($\sigma_{i,\phi} \leq 0.05$) for a "starmode" discharge, Figs. 2–4 indicate that $\eta_{\text{eff}} = 98\%$–99% is plausible for the device of Gu and Miley [10], provided that $\sigma_{e,\phi} \leq 0.002$. Of Figs. 5–7, Fig. 5 is the most appropriate for comparison to star-mode discharges. Fig. 5 indicates that η_{eff} could be as low as 96%, depending on the value of β. However, further comparison of the widths in Figs. 8–13 with [10] shows that there is no agreement. For instance, assuming that the local minima between the two peaks in a double peaked radial proton rate profile is located at the peak of the potential hill in a double potential well (see Fig. 1), then the structures in [10] have a width of $\sim$0.10. In Figs. 5–7 and Figs. 11–13, we can see that the widths of $\sim$0.10 only occur for Abs. DWDs much less than the target of 0.22.

This disagreement should not be a surprising outcome, considering that this paper focuses on the ideal case of a collisionless discharge, while the collisional phenomena in Gu and Miley's apparatus [10] make it unlikely that such high recirculation factors could have occurred in practice. In addition, there are rather large uncertainties in $\sigma_{i,\phi}$, $\sigma_{e,\phi}$, β, and P_i^c. Such a comparison may be considered futile, but it raises

the question of how such a deep double well could have been observed experimentally since the collisions would tend to smooth out large density perturbations. In that sense, the results presented here should be considered optimistic with respect to Abs. DWD due to the lack of collisions.

A possible explanation may be provided by Matsuura *et al.* [8]. These simulations show that a double radial proton peak can be generated without a double potential well ([8, Fig. 1] provides a good example). Although this model is also collisionless, it would seem that this result would be enough to cast a doubt on the claim made in [10], that a double peak in the radial proton rate profile is a "signature" of a double potential well structure. This does not prove that a double potential well was not observed in [10], but it raises the possibility that only a single potential well existed.

Another explanation could be made, considering that the collisional and noncollisional devices are different in nature. It was casually stated earlier that the collisions tend to smooth out the large density perturbation, but a detailed analysis would be needed to support this for the specific situation. If collisions push the electron distribution toward a Maxwellian, then the electrons in the cold tail may become trapped in the virtual anode, thus providing a source of electrons at the origin. It also seems intuitive that the collisions should degrade the ion recirculation factors. However, a mechanism is suggested in [10], by which relatively large recirculation factors can exist despite collisions. It is suggested that a type of collision that preserves the ion recirculation is a preferential charge exchange during the stationary part of an ion's orbit with a cold neutral.

REFERENCES

[1] R. M. Meyer, S. K. Loyalka, and M. A. Prelas, "Potential well structures in spherical inertial electrostatic confinement devices," *IEEE Trans. Plasma Sci.*, vol. 33, no. 4, pp. 1377–1394, Aug. 2005.

[2] I. Langmuir and K. E. Blodgett, "Currents limited by space charge between concentric spheres," *Phys. Rev.*, vol. 24, no. 1, pp. 49–59, Jul. 1924.

[3] R. L. Hirsch, "Inertial electrostatic confinement of ionized fusion gases," *J. Appl. Phys.*, vol. 38, no. 11, pp. 4522–4534, Oct. 1967.

[4] O. A. Lavrent'ev, *Investigation of an Electromagnetic Trap*, 1970. AEC-tr-7002.

[5] T. J. Dolan, "Electrostatic-inertial plasma confinement," Ph.D. dissertation, Univ. Illinois-Urbana–Champaign, Urbana, IL, 1975.

[6] D. A. Swanson, B. E. Cherrington, and J. T. Verdeyen, "Multiple potential-well structure created by electron injection in spherical geometry," *Appl. Phys. Lett.*, vol. 23, no. 3, pp. 125–126, Aug. 1973.

[7] D. A. Swanson, "Theoretical study of a spherical inertial electrostatic plasma confinement device," Ph.D. dissertation, Univ. Illinois-Urbana–Champaign, Urbana, IL, 1975.

[8] K. Matsuura, T. Takaki, Y. Nakao, and K. Kudo, "Radial profile of neutron production rate in spherical inertial electrostatic confinement plasmas," *Fus. Technol.*, vol. 39, no. 3, pp. 1167–1173, May 2001.

[9] H. Momota and G. H. Miley, "Virtual cathode in a stationary spherical inertial electrostatic confinement," *Fus. Sci. Technol.*, vol. 40, no. 1, pp. 56–65, Jul. 2001.

[10] Y. Gu and G. H. Miley, "Experimental study of potential structure in a spherical IEC fusion device," *IEEE Trans. Plasma Sci.*, vol. 28, no. 1, pp. 331–346, Feb. 2000.

[11] T. J. Dolan, J. T. Verdeyen, D. J. Meeker, and B. E. Cherrington, "Electrostatic-inertial plasma confinement," *J. Appl. Phys.*, vol. 43, no. 4, p. 1590, Apr. 1972.

[12] I. V. Tzonev, "Effect of large ion angular momentum spread and high current on inertial electrostatic confinement potential structures," M.S. thesis, Univ. Illinois-Urbana–Champaign, Urbana, IL, 1996.

Ryan M. Meyer (M'00) received the B.S. degree in electrical engineering and the M.S. degree in nuclear engineering from the University of Missouri-Columbia, Columbia, in 2002 and December 2004, respectively, where he is currently working toward the Ph.D. degree in nuclear engineering.

His research has been focused on theoretical and experimental studies of IEC devices.

Sudarshan K. Loyalka received the B.S. degree from University of Rajasthan, Rajasthan, India, in 1964, and the M.S. and Ph.D. degrees from Stanford University, Stanford, CA, in 1965 and 1967, respectively.

He is a Curators' Professor of nuclear engineering and chemical engineering with the University of Missouri-Columbia, Columbia. At the University of Missouri-Columbia, he has been the Director of their Particulate Systems Research Center since its inception in 1985. He has coauthored three books. His research and teaching interests are in the areas of aerosol mechanics, rarefied gas dynamics, and nuclear reactor physics and safety.

Dr. Loyalka was elected as a Fellow of the American Institute of Physics, in 1982, for his contributions to understandings of the role of gas-surface interactions on transport processes. He was also elected as a Fellow of the American Nuclear Society, in 1985, for his contributions to aerosol mechanics, transport theory, nuclear reactor physics and safety, and education of nuclear engineers. He received the David Sinclair Award of the American Association of Aerosol Research, in 1995, for his sustained outstanding research in aerosol science and technology, and the Glenn Murphy Award of the American Society for Engineering Education, in 1998, for education of nuclear engineers.

Mark A. Prelas (M'80) received the Ph.D. degree from the University of Illinois, Urbana–Champaign, in 1979.

He is an H. O. Croft Professor of nuclear engineering with the University of Missouri-Columbia, Columbia. He also worked with the U.S. Department of State in the Bureau of Arms Control from 1999 to 2000 and with the Idaho National Engineering Laboratory of the U.S. Department of Energy in 1987. He has worked in the areas of arms control for weapons of mass destruction, the strategic defense initiative, the development of nuclear, chemical and biological sensors, the synthesis and applications of wide bandgap materials, directed energy weapons, direct energy conversion, and gaseous electronics. He has published over 200 papers, five books and holds 12 national and international patents.

Dr. Prelas received the Presidential Young Investigator Award in 1984, was a Gas Research Institute Fellow in 1981, was a Fulbright Fellow at the University of New South Wales in 1992, was named a Fellow of the American Nuclear Society in 1999, and was a William C. Foster Fellow with the U.S. Department of State from 1999 to 2000.